Temporal coherence and correlation of counterpropagating twin photons

A. Gatti,[1,2] T. Corti,[2] and E. Brambilla[2]
[1]*Istituto di Fotonica e Nanotecnologie del CNR, Piazza Leonardo Da Vinci 32, D-Milano, Italy*
[2]*Dipartimento di Scienza e Alta Tecnologia dell' Università dell'Insubria, Via Valleggio 11, D-Como, Italy*
(Received 29 May 2015; published 4 November 2015)

This work analyzes the temporal coherence and correlation of counterpropagating twin photons generated in a quasiphase matched nonlinear crystal by spontaneous parametric down-conversion. We find out different pictures depending on the pump pulse duration relative to two characteristic temporal scales, determined, respectively, by the temporal separation between the counterpropagating and the co-propagating wave packets. When the pump duration is intermediate between the two scales, we show a transition from a highly entangled state to an almost separable state, with strongly asymmetric spectral properties of the photons.

DOI: 10.1103/PhysRevA.92.053809 PACS number(s): 42.65.Lm, 42.50.Ar, 42.50.Dv

I. INTRODUCTION

Spontaneous parametric down-conversion (SPDC) is one of the most accessible sources both of entangled photon pairs and of single photons, heralded by detection of the partner. The microscopic process, where a high energy photon of the pump laser splits into two lower energy photons, is ruled by conservation laws (energy, momentum, angular momentum, polarization), which are at the origin of a wide range of quantum correlations between the members of the pair.

In the standard co-propagating configuration, the two-photon state is characterized by a *high dimensional entanglement*, because a quantum correlation is present over huge temporal and angular bandwidths. The temporal correlation was historically the first one to be studied [1]: A down-conversion event can take place anywhere along the crystal, so that the arrival time of the twins is not known. However, the members of a pair, generated at the same point, propagate nearly in the same direction, and exit the crystal almost simultaneously. A small uncertainty in their temporal separation is present because of their different group velocities (type II) or because of the group velocity dispersion (type I), and can be reduced to the smallest limit (the optical cycle) when the spatial degrees of freedom are properly controlled [2,3]. Such a short correlation time results in a high-dimensional temporal entanglement [4]. Its spectral counterpart is the huge spectral bandwidth of SPCD emission, and the high dimensional spectral entanglement of SPDC photons [5]. High-dimensional entanglement offers relevant opportunities in view of broadband quantum communication schemes, but can also be regarded as a negative feature, because it affects the purity of heralded single photons.

This work considers a nonconventional configuration, where one of the down-converted photons is generated in the backward direction with respect to the pump laser, in a periodically poled crystal (Fig. 1). Although predicted almost 50 years ago [6], counterpropagating down-conversion has been only recently realized [7,8], thanks to technical advancements in achieving the submicrometer poling periods necessary to phase match the interaction [9].

Counterpropagating PDC presents unique features, as the presence of a threshold value of the pump intensity, beyond which coherent parametric oscillations take place [10], thereby the name *Mirrorless Optical parametric Oscillator* (MOPO) [7]. In a related work [11], we study the quantum correlation of counterpropagating twin beams close to the threshold; here, instead, we focus on the regime of spontaneous photon pairs production, well below threshold, and analyze the temporal quantum properties of counterpropagating twin photons generated in a purely collinear configuration.

A second peculiar feature of the MOPO is the narrow spectral bandwidth of emission (the backward-propagating wave can be more monochromatic than the pump laser [7]). In the quantum domain, as pointed out in [12], counterpropagating SPDC can generate highly monochromatic photon pairs in an almost separable state, which makes it a promising source of high-purity heralded single photons.

In this work we provide a detailed theoretical analysis of the effects of the spectral properties of the pump laser on the degree of entanglement of the state, identify the physical conditions under which the state may become separable, and provide a consistent interpretation of the transition from an entangled to a separable state.

In particular, we show that the system dynamics is governed by two well-separated time scales: a *long one*, related to the temporal separation of counterpropagating waves, which is on the order of the transit time of light along the crystal (tens of picoseconds), and a *short* one related to the temporal separation of co-propagating waves due to their different group velocities (order 1 ps or smaller). When the duration of the pump pulse is intermediate between the two scales, we show that the state becomes separable, and remains separable for a wide range of pump durations. Conversely, it has a high degree of entanglement in the two opposite limits. Notice that such a difference of time scales occurs naturally in the counterpropagating configuration, for basically any kind of material and tuning condition. This is quite different from the co-propagating case where separability of the state requires special operational points [13].

In addition, we shall investigate the coherence properties of the SPDC photons taken individually, showing a transition from a symmetric state, for a long pump pulse, to a highly asymmetric state for a short pump pulse. In particular, in the regime where the state is separable, the spectrum of the signal turns out to reproduce the spectrum of the co-propagating pump laser, while that of the backward-propagating idler is entirely determined by the crystal properties.

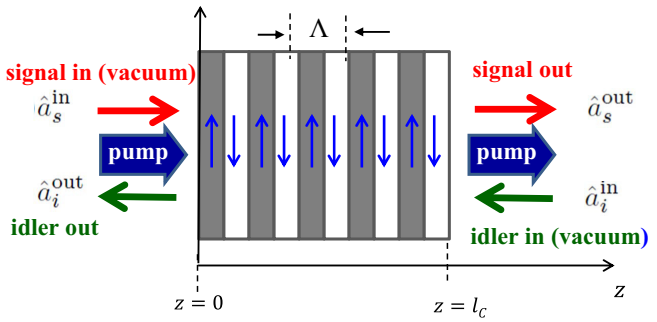

FIG. 1. (Color online) Geometry of the counterpropagating down-conversion (see text).

The paper is organized as follows: Section II introduces a quantum model for counterpropagating PDC; Sec. III characterizes the quantum correlation of twin photons in the spectral domain, while Sec. IV gives an interpretation of the transition from entanglement to separability by analyzing the correlation in the temporal domain. Section V is devoted to the coherence properties of twin photons. Finally, Sec. VI quantifies the degree of entanglement of the state via the Schmidt number.

II. THE MODEL

The starting point of our analysis are the equations describing the propagation of three interacting pump, signal, and idler waves along a slab of periodically poled second-order nonlinear crystal (Fig. 1). We consider here only collinear propagation, either assuming that light is collected at small propagation angles with respect to the pump, or because of a waveguiding configuration. In a crystal with periodic inversion of the nonlinear susceptibility, the momentum conservation in the three-wave interaction is replaced by a less restrictive law (quasiphase matching) [14], which includes also the momenta $\frac{2\pi}{\Lambda}m$ of the nonlinear lattice, where Λ is the poling period (for example, $m = \pm 1, \pm 3 \ldots$ for a simple poling). Since the effective nonlinearity is higher for lower orders, one usually tries to phase match the first order $m = \pm 1$ interaction. The counterpropagating configuration (Fig. 1), in which one wave—say the idler—is generated in the backward direction with respect to the pump laser, thus requires a poling period on the order of the pump wavelength, because the pump momentum needs to be almost entirely compensated by the grating momentum $k_G = \frac{2\pi}{\Lambda}$. In these conditions, the central frequencies ω_s, $\omega_i = \omega_p - \omega_s$ of the down-converted wave packets are determined by quasiphase matching at the central pump frequency ω_p,

$$k_{0s} - k_{0i} = k_{0p} - \frac{2\pi}{\Lambda}, \tag{1}$$

where $k_{0j} = n_j(\omega_j)\omega_j/c$, $j = s,i,p$ are the wave numbers at the three central frequencies. We shall mostly focus on the commonly realized type O interaction [7], where the three waves have the same polarization, but we leave the formalism quite general. Hence the subscript j in the wave number may refer to dispersion relations for either the ordinary or extraordinary wave, including thus type II or I PDC.

Next, we introduce the positive frequency part of field operators (with dimension of photon destruction operators) for the three wave packets as

$$\hat{A}_s(\Omega,z) = e^{+ik_s(\Omega)z}\hat{a}_s(\Omega,z), \tag{2a}$$

$$\hat{A}_i(\Omega,z) = e^{-ik_i(\Omega)z}\hat{a}_i(\Omega,z), \tag{2b}$$

$$\hat{A}_p(\Omega,z) = e^{+ik_p(\Omega)z}\hat{a}_p(\Omega,z), \tag{2c}$$

where capital Ω is a frequency offset from the carrier frequencies, and $k_j(\Omega)$ are the wave numbers at frequency $\omega_j + \Omega$. In this definition, the factors $e^{\pm ik_j(\Omega)z}$ account for all the effects of the linear propagation along the medium. Hence the operators $\hat{a}_j$ have a slow variation along the crystal because they evolve only under the effects of the nonlinear interaction. Their coupled equations of propagation can thus be written as (see [11] for a more detailed analysis)

$$\frac{\partial}{\partial z}\hat{a}_s(\Omega,z) = \chi \int d\Omega' \hat{a}_p(\Omega+\Omega',z)\hat{a}_i^\dagger(\Omega',z)e^{-i\mathcal{D}(\Omega,\Omega')z}, \tag{3a}$$

$$\frac{\partial}{\partial z}\hat{a}_i(\Omega,z) = -\chi \int d\Omega' \hat{a}_p(\Omega+\Omega',z)\hat{a}_s^\dagger(\Omega',z)e^{-i\mathcal{D}(\Omega',\Omega)z}, \tag{3b}$$

$$\frac{\partial}{\partial z}\hat{a}_p(\Omega,z) = -\chi \int d\Omega' \hat{a}_s(\Omega',z)\hat{a}_i(\Omega-\Omega',z)e^{i\mathcal{D}(\Omega,\Omega-\Omega')z}, \tag{3c}$$

where χ is proportional to the effective second-order susceptibility of the crystal, and only the first-order terms ± 1 in the Fourier expansion of the periodic nonlinear susceptibility have been retained (namely order -1 for signal and idler, order $+1$ for the pump). In these equations,

$$\mathcal{D}(\Omega,\Omega') = k_s(\Omega) - k_i(\Omega') - k_p(\Omega+\Omega')' + \frac{2\pi}{\Lambda} \tag{4}$$

is the effective phase mismatch that rules the efficiency of each elementary down-conversion process, where a signal and an idler photon of frequencies $\omega_s + \Omega$, $\omega_i + \Omega'$ are generated out of a pump photon of frequency $\omega_p + \Omega + \Omega'$. Notice that, apart from the different form of the phase matching (4), the only formal difference with the usual co-propagating case (see, e.g., [15]) is the minus sign appearing at the right-hand side of (3b) for the counterpropagating idler. As we shall see, however, this minus sign leads to very relevant physical differences.

A. Low-gain limit

In a parent work [11], we analyze these equations for a generic gain, including the region close to the MOPO threshold. This work, instead, focuses on the ultralow gain regime, much below the MOPO threshold, where photons pairs are generated by purely spontaneous down-conversion. In this regime, the depletion of the pump beam can be neglected and the pump approximated by a constant c-number field, corresponding to the pump pulse at the crystal input face,

$$\hat{a}_p(\Omega,z) \to \alpha_p(\Omega,z) \approx \alpha_p(\Omega,z=0). \tag{5}$$

The strength of the parametric coupling is then described by the dimensionless gain parameter,

$$g = \sqrt{2\pi}\,\chi\alpha_p(t=0)l_c, \tag{6}$$

where $\alpha_p(t=0)$ is the peak value of the pump temporal profile. Notice that in the limit of a monochromatic pump [11,16] $g = \pi/2$ represents the threshold for the MOPO. Conversely, in the limit $g \ll 1$ Eq. (3) can be solved perturbatively. Namely, we write the formal solution of (3), starting from the boundary conditions:

$$\hat{a}_s(\Omega, z=0) = \hat{a}_s^{\rm in}(\Omega), \tag{7}$$

$$\hat{a}_i(\Omega, z=l_c) = \hat{a}_i^{\rm in}(\Omega), \tag{8}$$

determined by the input signal and idler fields, entering the crystal from the left face at $z=0$ and from the right face at $z=l_c$, respectively (Fig. 1). By solving iteratively, a perturbative series of powers of g is obtained. By keeping only the first-order terms in $g \ll 1$, one obtains a Boguliobov linear transformation that links the output to the input operators:

$$\begin{aligned}\hat{a}_s^{\rm out}(\Omega_s) &= \hat{a}_s(\Omega_s, z=l_c)\\ &= \hat{a}_s^{\rm in}(\Omega_s) + \int d\Omega_i\,\psi(\Omega_s,\Omega_i)\hat{a}_i^{\rm in\dagger}(\Omega_i), \qquad (9a)\\ \hat{a}_i^{\rm out}(\Omega_i) &= \hat{a}_i(\Omega_s, z=0)\\ &= \hat{a}_i^{\rm in}(\Omega_i) + \int d\Omega_s\,\psi(\Omega_s,\Omega_i)\hat{a}_s^{\rm in\dagger}(\Omega_s), \qquad (9b)\end{aligned}$$

where

$$\psi(\Omega_s,\Omega_i) = \frac{g}{\sqrt{2\pi}}\tilde{\alpha}_p(\Omega_s+\Omega_i) \times \mathrm{sinc}\left[\frac{\mathcal{D}(\Omega_s,\Omega_i)l_c}{2}\right] e^{-i\frac{\mathcal{D}(\Omega_s,\Omega_i)l_c}{2}} \tag{10}$$

is the so-called *biphoton amplitude*. Here

$$\tilde{\alpha}_p(\Omega) = \int \frac{dt}{\sqrt{2\pi}} e^{i\Omega t}\frac{\alpha(t)}{\alpha_p(t=0)} \tag{11}$$

is the Fourier profile of the pump pulse at the crystal input face, normalized to its temporal peak value. Notice that Eq. (9) defines a unitary transformation only up to first order in g. In the following, the input signal and idler field at the left and right end faces of the crystal will be taken in the vacuum state.

It is worth remarking that the quantum-field formalism here employed can be replaced by a state formalism (see also [17]), where the state evolves under the parametric interaction instead of the field operators. By finding the generator of the transformation (9), applying it to the input vacuum state, and retaining terms up to first order in the gain $g \ll 1$ (see Appendix B for details), one obtains

$$|\phi\rangle_{\rm out} = |0\rangle + \int d\Omega_s d\Omega_i\,\psi(\Omega_s,\Omega_i)\hat{a}_s^\dagger(\Omega_s)\hat{a}_i^\dagger(\Omega_i)|0\rangle. \tag{12}$$

This is the well-known biphoton state, describing the superposition of the vacuum state $|0\rangle$ and of a two-photon state, where the photon pair can be generated in any of the Fourier modes Ω_s,Ω_i with probability amplitude $\psi(\Omega_s,\Omega_i)$. In this respect, the formalism used here can be connected to the one employed in [12,18].

III. SPECTRAL BIPHOTON CORRELATION

This section is devoted to the biphoton correlation in the spectral domain. Precisely, we focus on the field correlation $\langle\hat{A}_s^{\rm out}(\Omega_s)\hat{A}_i^{\rm out}(\Omega_i)\rangle$, proportional to the probability amplitude of finding a pair of photons at frequencies Ω_s,Ω_i at the crystal output faces. Using the input-output relations (9) and the definitions (2):

$$\left\langle\hat{A}_s^{\rm out}(\Omega_s)\hat{A}_i^{\rm out}(\Omega_i)\right\rangle = e^{ik_s(\Omega_s)l_c}\psi(\Omega_s,\Omega_i), \tag{13}$$

with ψ given by Eq. (10). As usual, the biphoton correlation is the product of two terms: (i) the pump spectral amplitude $\tilde{\alpha}_p(\Omega_s+\Omega_i)$, reflecting the energy conservation in the microscopic process, and (ii) the phase matching function $\mathrm{sinc}(\mathcal{D}l_c/2)e^{-i\mathcal{D}l_c/2}$, reflecting the generalized momentum conservation. Concerning the latter, we can expand $\mathcal{D}(\Omega_s,\Omega_i)$ in Eq. (4) in power series of the frequency shifts from the carriers. Down-conversion spectra are typically narrow [7,8], as will become clear in the following, so that one is allowed to retain only terms up to first order in Ω_s, Ω_i,

$$\begin{aligned}\mathcal{D}(\Omega_s,\Omega_i)\frac{l_c}{2} &\approx \frac{l_c}{2}[(k_s'-k_p')\Omega_s - (k_i'+k_p')\Omega_i] \qquad (14)\\ &= -\left(\frac{\Omega_s}{\Omega_{\rm gvm}} + \frac{\Omega_i}{\Omega'_{\rm gvs}}\right), \qquad (15)\end{aligned}$$

where the zero-order term vanishes because of Eq. (1), and $k_j' = dk_j/d\omega|_{\omega=\omega_j}$, $j=s,i,p$. We thus see the appearance of the two characteristic temporal scales:

$$\tau_{\rm gvm} := \Omega_{\rm gvm}{}^{-1} = \frac{1}{2}\left[\frac{l_c}{v_{gp}} - \frac{l_c}{v_{gs}}\right], \tag{16}$$

$$\tau'_{\rm gvs} := \Omega'_{\rm gvs}{}^{-1} = \frac{1}{2}\left[\frac{l_c}{v_{gp}} + \frac{l_c}{v_{gi}}\right], \tag{17}$$

where $v_{gj} = 1/k_j'$ are the group velocities of the three wave packets at the central frequencies. The first scale in Eq. (16) describes the "small" temporal separation between the co-propagating waves due to their group velocity mismatch (GVM). The second one in Eq. (17) accounts for the "large"temporal separation of the counterpropagating pump and idler waves, which is ruled by the time needed by the pulse centers to cross the crystal. Closely related,

$$\tau_{\rm gvs} = \Omega_{\rm gvs}{}^{-1} = \frac{1}{2}\left[\frac{l_c}{v_{gs}} + \frac{l_c}{v_{gi}}\right], \tag{18}$$

describes the characteristic separation of the arrival times of an idler and a signal photon at their exit faces. Clearly, since group velocities are close, $\tau_{\rm gvs} \approx \tau'_{\rm gvs}$, while $\tau_{\rm gvm} \ll \tau'_{\rm gvs}, \tau_{\rm gvs}$, and

$$\eta = \frac{\tau_{\rm gvm}}{\tau'_{\rm gvs}} = \frac{\Omega'_{\rm gvs}}{\Omega_{\rm gvm}} \ll 1. \tag{19}$$

Therefore, the phase matching has two well-separated scales of variation: As a function of the signal frequency it decays on the broad bandwidth $\Omega_{\rm gvm}$, while as a function of the idler

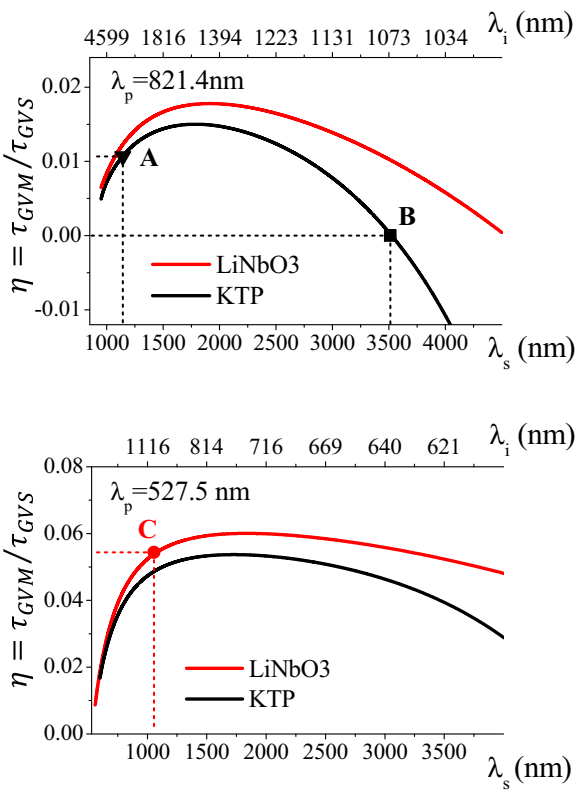

FIG. 2. (Color online) Ratio $\eta = \tau_{\rm gvm}/\tau'_{\rm gvs}$ for periodically poled KTP and $LiNbO_3$, pumped in the infrared or visible, for type 0 $e \to ee$ down-conversion. Point **A** is KTP pumped at $\lambda_p = 821$ nm, with $\Lambda_{\rm pol} = 800$ nm, $\lambda_s = 1141$ nm, $\lambda_i = 2932$ nm, corresponding to the experiment in [7]; **B** is the zero GVM point for the KTP at $\lambda_p = 821$ nm, corresponding to $\Lambda_{\rm pol} = 290$ nm, $\lambda_s = 3523$ nm, $\lambda_i = 1071$ nm. **C** is a $LiNbO_3$ slab pumped at $\lambda_p = 527.5$ nm, for degenerate PDC at $\lambda_s = \lambda_i = 1055$ nm, with $\Lambda_{\rm pol} = 236$ nm.

frequency it decays on the narrow bandwidth $\Omega'_{\rm gvs}$. Plots of the parameter η, for periodically poled KTP (potassium titanyl phosphate) and $LiNbO_3$ (lithium niobate), are shown in Fig. 2, where **A,B,C** are the points that will be used as examples in the following.

Finally, a third relevant scale is the pump spectral bandwidth. For a coherent Gaussian pump $\alpha_p(t) = \alpha_p(0)\exp(-\frac{t^2}{2\tau_p^2})$, the pulse duration τ_p is the inverse of the bandwidth,

$$\tau_{\rm p} = \frac{1}{\Delta\Omega_{\rm p}}. \tag{20}$$

Depending on the pump bandwidth relative to the spectral scales of phase matching, different physical situations arise. The three relevant possibilities, depicted in Fig. 3, will be studied separately in the following.

(i) Limit of a CW pump

We assume a narrowband pump pulse, such that

$$\tau_p \gg \tau'_{\rm gvs} \gg \tau_{\rm gvm}, \quad \text{or} \quad \Delta\Omega_{\rm p} \ll \Omega'_{\rm gvs} \ll \Omega_{\rm gvm}. \tag{21}$$

This limit corresponds to a pump pulse that in the z direction is much longer than the crystal slab, and for a crystal of some mm length requires a pulse duration of hundreds of picoseconds or longer. In this limit the pump spectral profile $\tilde{\alpha}_p(\Omega_s + \Omega_i)$ is much narrower than the phase matching bandwidths, and the geometry of the correlation is dominated by energy conservation, which requires that the twins are generated at symmetric frequencies $\Omega_s + \Omega_i = \Omega_p \approx 0$. As a consequence, the biphoton correlation (10) has a sharp maximum along the diagonal $\Omega_s = -\Omega_i$, as shown by Fig. 3(a). Indeed, as derived in Appendix A, in this limit the correlation is well approximated by

$$\psi(\Omega_s,\Omega_i) \simeq \frac{g}{\sqrt{2\pi}}\tilde{\alpha}_p(\Omega_s+\Omega_i)\,\mathrm{sinc}\left(\frac{\Omega_s}{\Omega_{\rm gvs}}\right)e^{-i\frac{\Omega_s}{\Omega_{\rm gvs}}} \tag{22}$$

$$\simeq \frac{g}{\sqrt{2\pi}}\tilde{\alpha}_p(\Omega_s+\Omega_i)\,\mathrm{sinc}\left(\frac{\Omega_i}{\Omega_{\rm gvs}}\right)e^{i\frac{\Omega_i}{\Omega_{\rm gvs}}}. \tag{23}$$

(ii) Limit of an ultrashort pump pulse

We consider here the limit:

$$\tau_p \ll \tau_{\rm gvm}, \tau'_{\rm gvs}, \quad \text{or} \quad \Delta\Omega_{\rm p} \gg \Omega_{\rm gvm}, \Omega'_{\rm gvs}, \tag{24}$$

where the pump pulse is not only shorter than the crystal length, but also shorter than the average separation between the pump and signal wave packets due their GVM. In our

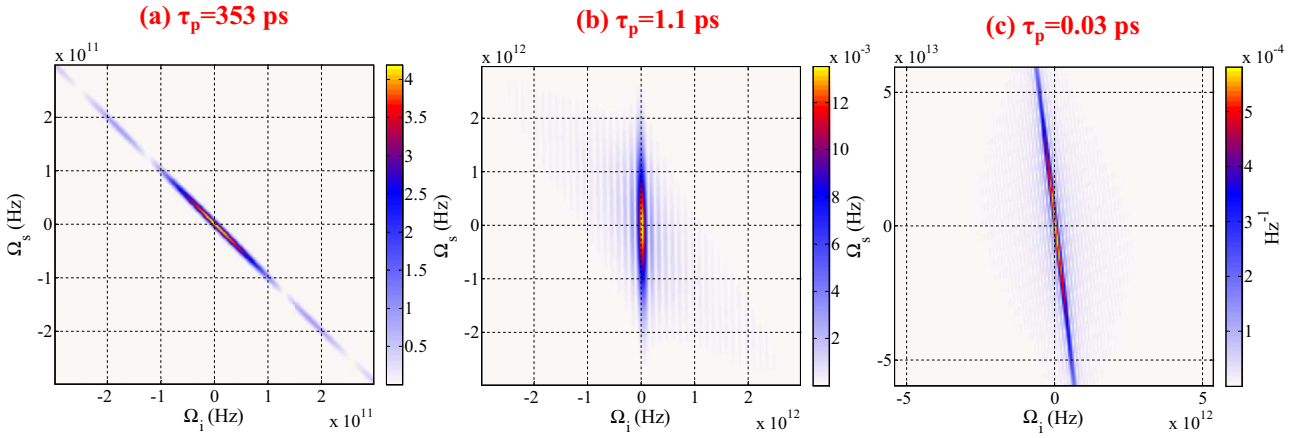

FIG. 3. (Color online) Biphoton correlation $|\psi|$ [Eq. (10)] in the plane (Ω_i,Ω_s), in various pumping regimes. Example of a 4-mm PPKTP, pumped at 821.4 nm, corresponding to the point **A** in Fig. 2, with $\tau'_{\rm gvs} = 25.2$ ps, $\tau_{\rm gvm} = 0.27$ ps. (a) Quasi-CW pump pulse $\tau_{\rm p} = 253$ ps. (b) Intermediate pump pulse $\tau_p = 1.1$ ps. (c) Ultrashort pump $\tau_{\rm p} = 0.03$ ps. Note the different scales of the plots $10^{11} \to 10^{13}$ Hz.

examples this corresponds to duration shorter than 100 fs. In these conditions, the pump spectral profile $\tilde{\alpha}_p(\Omega_s+\Omega_i)$ decays slowly with respect to $\mathrm{sinc}\mathcal{D}(\Omega_s,\Omega_i)l_c/2$, so that the geometry of the biphoton correlation is dominated by the phase matching, i.e., by the momentum conservation. As a result [Fig. 3(c)] the biphoton correlation takes the approximated form,

$$\psi(\Omega_s,\Omega_i) \simeq \frac{g}{\sqrt{2\pi}}\tilde{\alpha}_p[\Omega_s(1-\eta)]\mathrm{sinc}\left(\frac{\Omega_s}{\Omega_{\mathrm{gvm}}}+\frac{\Omega_i}{\Omega'_{\mathrm{gvs}}}\right) \times e^{i\left(\frac{\Omega_s}{\Omega_{\mathrm{gvm}}}+\frac{\Omega_i}{\Omega'_{\mathrm{gvs}}}\right)} \tag{25}$$

$$\simeq \frac{g}{\sqrt{2\pi}}\tilde{\alpha}_p\left[-\Omega_i\frac{1-\eta}{\eta}\right]\mathrm{sinc}\left(\frac{\Omega_s}{\Omega_{\mathrm{gvm}}}+\frac{\Omega_i}{\Omega'_{\mathrm{gvs}}}\right) \times e^{i\left(\frac{\Omega_s}{\Omega_{\mathrm{gvm}}}+\frac{\Omega_i}{\Omega'_{\mathrm{gvs}}}\right)}. \tag{26}$$

When plotted in the plane (Ω_i,Ω_s), the function shows a sharp maximum along the line,

$$\Omega_s = -\Omega_i\frac{\Omega_{\mathrm{gvm}}}{\Omega'_{\mathrm{gvs}}}, \tag{27}$$

where phase matching occurs [see Eq. (15)], and very asymmetric spectral properties of the signal -idler photons.

(iii) Intermediate pump pulse

The intermediate case, where

$$\tau'_{\mathrm{gvs}} \gg \tau_p \gg \tau_{\mathrm{gvm}}, \quad \text{or} \quad \Omega'_{\mathrm{gvs}} \ll \Delta\Omega_{\mathrm{p}} \ll \Omega_{\mathrm{gvm}}, \tag{28}$$

is the most peculiar one, because the biphoton correlation may approach a separable function of Ω_s,Ω_i [Fig. 3(b)]. First of all, we remark that the limit (28) is strictly realized only for $\eta=\tau_{\mathrm{gvm}}/\tau'_{\mathrm{gvs}}\to 0$, i.e., for a vanishing group velocity mismatch between the pump and the signal. This condition is favorable to separability, because as $\eta\to 0$ the phase matching function tends to become a stripe parallel to the Ω_s axis [see Eq. (27)], but it is not a sufficient one, because of the role of the pump profile in Eq. (10). However, provided that the pump spectrum satisfies the intermediate limit (28), it can be demonstrated (Appendix A) that the biphoton amplitude (10) approaches the factorized form:

$$\psi(\Omega_s,\Omega_i) \to \frac{g}{\sqrt{2\pi}}\tilde{\alpha}_p(\Omega_s)e^{i\frac{\Omega_s}{\Omega_{\mathrm{gvm}}}}\ \mathrm{sinc}\left(\frac{\Omega_i}{\Omega_{\mathrm{gvs}}}\right)e^{i\frac{\Omega_i}{\Omega'_{\mathrm{gvs}}}}, \tag{29}$$

i.e., it becomes the product of a function of Ω_s, reproducing the pump profile, and a function of Ω_i, corresponding to the phase matching profile. This describes a nonentangled biphoton state, with the signal photon generated in the same spectro-temporal mode as the pump, while the spectral mode of the idler is dictated by the phase matching "sinc" function of width Ω_{gvs}.

This qualitative picture will be confirmed by the evaluation of the Schmidt number in Sec. VI, and will be interpreted and discussed in the light of the temporal correlation of biphotons in the next section.

IV. INTERPRETATION: THE BIPHOTON CORRELATION IN THE TEMPORAL DOMAIN

An alternative insight into the issue of separability vs entanglement is provided by the analysis of the biphoton correlation in the temporal domain. We consider

$$\phi(t_s,t_i) = \left\langle \hat{A}_s^{\mathrm{out}}(t_s)\hat{A}_i^{\mathrm{out}}(t_i)\right\rangle = \int\frac{d\Omega_s}{\sqrt{2\pi}}\int\frac{d\Omega_i}{\sqrt{2\pi}}e^{-i(\Omega_s t_s+\Omega_i t_i)}e^{ik_s(\Omega_s)l_c}\psi(\Omega_s,\Omega_i), \tag{30}$$

which is proportional to the probability amplitude of finding a signal and an idler photon at their crystal end faces at times t_s,t_i.

By using the linear approximation for phase matching (15) and performing the simple Fourier transformations involved in (30) we obtain

$$\phi(\bar{t}_s,\bar{t}_i) = \frac{ge^{ik_s l_c}}{2\tau_{\mathrm{gvs}}}\alpha_p\left(\bar{t}_s+\eta\frac{\bar{t}_s-\bar{t}_i}{1-\eta}\right)\mathrm{Rect}\left(\frac{\bar{t}_s-\bar{t}_i}{2\tau_{\mathrm{gvs}}}\right), \tag{31}$$

where

$$\mathrm{Rect}(x) = \begin{cases}1 & \text{for} \quad x\in\left(-\frac{1}{2},\frac{1}{2}\right)\\ 0 & \text{elsewhere}\end{cases} \tag{32}$$

is the box function of unitary width. The barred arguments $\bar{t}_s,\bar{t}_i$ denote time intervals measured starting from the arrival times of the centers of the signal and idler wave packets. Precisely, $\bar{t}_{s,i}=t_{s,i}-t_{As,i}$, where

$$t_{As} = (k'_s+k'_p)\frac{l_c}{2} = t_{Ap}-(k'_p-k'_s)\frac{l_c}{2}, \tag{33}$$

$$t_{Ai} = (k'_i+k'_p)\frac{l_c}{2} = t_{Ap}-(k'_p-k'_i)\frac{l_c}{2}, \tag{34}$$

where $t_{Ap}=k'_p l_c$ is the time when the center of the pump pulse exits the crystal slab. Figure 4 shows three examples of the temporal correlation function (31).

The general formula (31) simplifies in the limit of a pump long with respect to τ_{gvm}, i.e., in the quasi-CW or intermediate limits (21), (28):

$$\phi(\bar{t}_s,\bar{t}_i) \overset{\tau_p\gg\tau_{\mathrm{GVM}}}{\simeq} ge^{ik_s l_c}\alpha_p(\bar{t}_s)\frac{1}{2\tau_{\mathrm{gvs}}}\mathrm{Rect}\left(\frac{\bar{t}_i-\bar{t}_s}{2\tau_{\mathrm{gvs}}}\right). \tag{35}$$

Indeed, for a pump pulse long with respect to τ_{gvm}, one has $\alpha_p(\bar{t}_s+\eta\frac{\bar{t}_s-\bar{t}_i}{1-\eta})\approx\alpha_p(\bar{t}_s)$, because $|\bar{t}_s-\bar{t}_i|$ is limited by the box function to values smaller than τ_{gvs}, so that $\eta\frac{|\bar{t}_s-\bar{t}_i|}{1-\eta} = \frac{\tau_{\mathrm{gvm}}}{\tau_{\mathrm{gvs}}}|\bar{t}_s-\bar{t}_i| \leqslant \tau_{\mathrm{gvm}} \ll \tau_p$.

Formula (35) shows that in the limit of a negligible GVM, the distribution of separations $\bar{t}_s-\bar{t}_i$ between the arrival times of the twin photons is entirely described by the box function of half-width τ_{gvs}, which roughly corresponds to the *long* transit time of light along the crystal slab. As already noticed in [16], this is a noteworthy difference with the copropagating case, where the uncertainty in the temporal separation of the twins is short, because determined at most by the group velocity dispersion or mismatch along the crystal. This long correlation is at the origin of the narrow frequency bandwidth of the counterpropagating scheme (see also Sec. V), in sharp contrast with the huge bandwidth of the standard configuration.

The form (35) of the temporal correlation clearly reflects the spontaneous character of the process, where photon pairs can be generated at any point of the crystal with uniform probability. Thus, assuming for simplicity that the twins

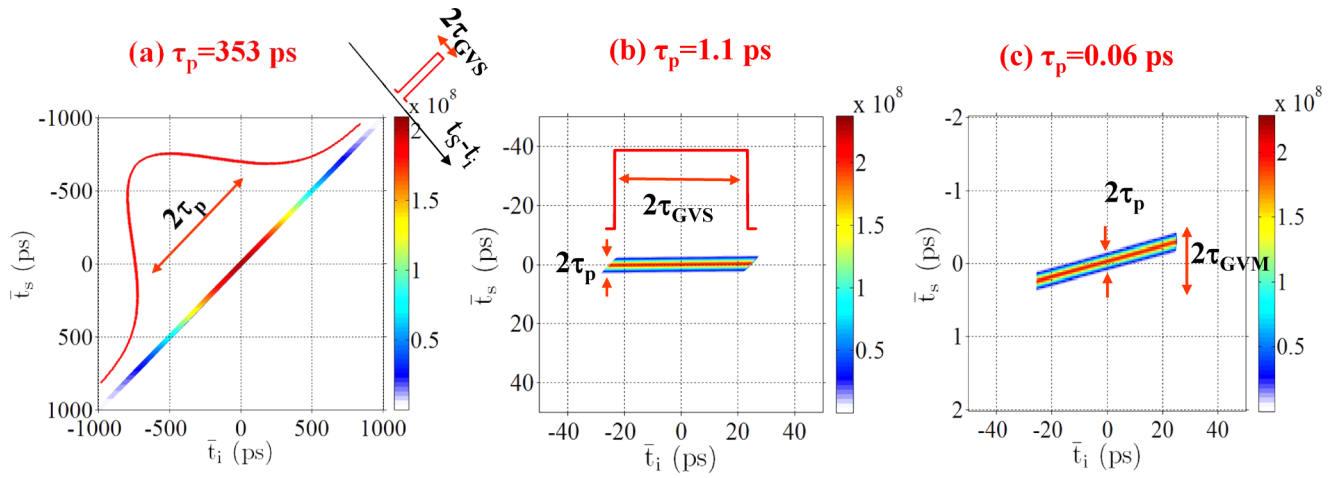

FIG. 4. (Color online) Temporal correlation of twin photons $|\phi(\bar{t}_i,\bar{t}_s)|$, given by Eq. (31), plotted in the plane $(\bar{t}_i,\bar{t}_s)$. (a) High entanglement case, with $\mathcal{K} \simeq 26$, for a quasi-CW pump $\tau_p = 14\tau'_{gvs}$. (b) Almost separable case with $\mathcal{K} \simeq 1.06$, for an intermediate pump $\tau_p = 0.04\tau'_{gvs} = 4\tau_{gvm}$. (c) Ultrashort pulse $\tau_p = 0.22\tau_{gvm}$, corresponding to an entangled state with $\mathcal{K} \simeq 4$. Same KTP crystal as in Fig. 6.

travel with the same group velocities $v_{gs} = v_{gi}$, the separation between their arrival times ranges with uniform probability from zero, when the two photons are generated at the center of the crystal up to $\pm\tau_{gvs} = l_c/v_g$, when they are generated at each of the end faces.[1]

The CW pump limit [Fig. 4(a)] corresponds to the situation where the pump pulse is much longer than the possible temporal separation τ_{gvs} of the twins. In this case, the usual picture of the temporal entanglement of twin photons holds: The time when a signal or idler photon is individually detected has a large undeterminacy, because a photon pair can be generated at any time along the pump pulse. However, from the arrival time of one member of the pair one can infer the arrival time of the other with a much smaller uncertainty τ_{gvs}, which represents the mean uncertainty in the arrival time of one photon provided its twin hs been detected, i.e., the *correlation time*. This kind of correlation is basically what was predicted in Ref. [16] for a strictly monochromatic pump.

However, when the pump pulse shortens below τ_{gvs} [Fig. 4(b)] this description ceases to be valid, because the localization of the pump pulse provides an absolute timing information of the arrival of the signal, more precise than the uncertainty in the temporal separation of the twins. Indeed when the pump pulse is much shorter than τ_{gvs}, but still long enough that GVM is negligible, the signal wave packet overlaps almost exactly with the pump pulse during propagation, and the uncertainty in the arrival time of the signal is just the pulse duration. This is much smaller than the conditional uncertainty τ_{gvs} by which the arrival time of the idler can be inferred from that of the signal. As a consequence, the exit times of the twins appear to be completely uncorrelated. Indeed, the temporal correlation in Fig. 4(b) is, approximately,

$$\phi(\bar{t}_s,\bar{t}_i) \simeq g e^{ik_s l_c}\alpha_p(\bar{t}_s)\frac{1}{2\tau_{gvs}}\mathrm{Rect}\left(\frac{\bar{t}_i}{2\tau_{gvs}}\right), \tag{36}$$

which is a factorable function of $\bar{t}_s,\bar{t}_i$.

Notice that when the pump pulse is so short that GVM starts to be important [Fig. 4(c)], there is again a loss of absolute timing information. In this case, the arrival time of the signal cannot be inferred from that of the pump with a precision better than τ_{gvm}. In contrast, the arrival time of the signal *conditioned* to a photon count in the idler arm can be predicted within the short pump duration τ_p, and the state becomes again entangled. This can be better understood by looking at the correlation function (31), which for $\tau_p \ll \tau_{gvm}$ can be rewritten as

$$\phi(\bar{t}_s,\bar{t}_i) = \frac{g e^{ik_s l_c}}{2\tau_{gvs}}\alpha_p\left(\frac{\bar{t}_s-\eta\bar{t}_i}{1-\eta}\right)\mathrm{Rect}\left(\frac{\bar{t}_s-\bar{t}_i}{2\tau_{gvs}}\right) \tag{37}$$

$$\simeq \frac{g e^{ik_s l_c}}{2\tau_{gvs}}\alpha_p\left(\frac{\bar{t}_s-\eta\bar{t}_i}{1-\eta}\right)\mathrm{Rect}\left(\frac{\bar{t}_s}{2\tau_{gvm}}\right), \tag{38}$$

where the last line has been obtained by substituting $\bar{t}_i = \bar{t}_s/\eta$ inside the argument of the box function (valid because the pump profile is much narrower than both τ_{gvs} and τ_{gvm}). From formula (38) we see that, provided that an idler photon is detected at time $\bar{t}_i$, the arrival time of the signal can be predicted as $\bar{t}_s = \eta\bar{t}_i$ within the narrow uncertainty of the pump duration τ_p [see also Fig. 4(c)]. However, when the idler is not detected, the overall uncertainty in the signal arrival time is the larger width τ_{gvm} of the box function. Clearly this argument predicts an entangled state, with the number of modes scaling as τ_{gvm}/τ_p, in agreement with the results for the Schmidt number that will be presented in Sec. VI [see Eq. (62)].

V. SPECTRAL COHERENCE OF COUNTERPROPAGATING PHOTONS

This section is devoted to the marginal statistics of individual signal and idler photons. The focus is on their spectral

[1]Precisely, when the two photons are generated at the crystal center $t_s - t_i = t_{As} - t_{Ai} = (k'_s - k'_i)l_c/2 \approx 0$, and the delay between their arrival times ranges uniformly between (i) $t_s - t_i = t_{As} - t_{Ai} - \tau_{gvs} = -k'_i l_c$, when they are generated at the right end face of the slab, and (ii) $t_s - t_i = t_{As} - t_{Ai} + \tau_{gvs} = k'_s l_c$ when the photon pair is generated at the left end face.

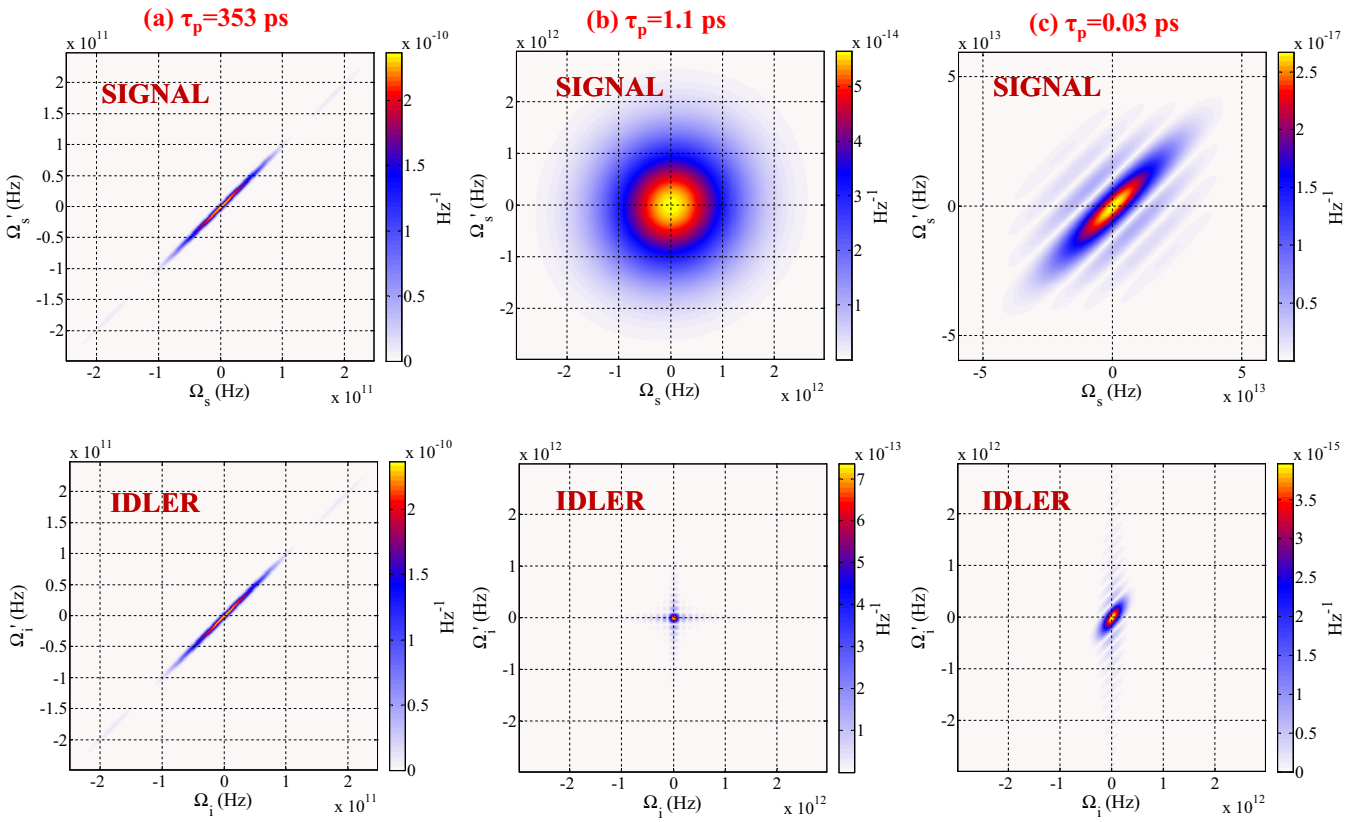

FIG. 5. (Color online) The coherence functions $|G(\Omega,\Omega')|$ of the forward signal and backward-propagating idler are plotted in the upper and lower row, respectively, for different pumping regime. (a) Quasi-CW pump pulse $\tau_p = 353$ ps. (b) Intermediate pump pulse $\tau_p = 1.1$ ps. (c) Ultrashort pump $\tau_p = 0.03$ ps. Same KTP crystal slab as in Fig. 3 (point **A** in Fig. 2), with $\tau'_{gvs} = 25.2$ ps, $\tau_{gvm} = 0.27$ ps. Note the different scales in the panels.

coherence properties, studied by means of the first-order coherence functions,

$$G_s^{(1)}(\Omega,\Omega') = e^{-i[k_s(\Omega')-k_s(\Omega)]l_c}\langle \hat{A}_s^{\dagger\,\mathrm{out}}(\Omega)\hat{A}_s^{\mathrm{out}}(\Omega')\rangle,$$
$$G_i^{(1)}(\Omega,\Omega') = \langle \hat{A}_i^{\dagger\,\mathrm{out}}(\Omega)\hat{A}_i^{\mathrm{out}}(\Omega')\rangle, \quad (39)$$

(where a propagation phase factor is present in the first definition just for convenience of notation). From the input-output relations (9) one has

$$G_s^{(1)}(\Omega_s,\Omega'_s) = \int d\Omega_i\, \psi^*(\Omega_s,\Omega_i)\psi(\Omega'_s,\Omega_i), \quad (40)$$
$$G_i^{(1)}(\Omega_i,\Omega'_i) = \int d\Omega_s\, \psi^*(\Omega_s,\Omega_i)\psi(\Omega_s,\Omega'_i), \quad (41)$$

i.e., the coherence functions are convolution integrals over the biphoton amplitude ψ, given by Eq. (10). The knowledge of the $G_j^{(1)}$ is sufficient to determine all the statistical properties of the marginal distributions. For example, the autocorrelation of the light intensities $\hat{I}_j = \hat{A}_j^\dagger \hat{A}_j$,

$$\langle \hat{I}_j(\Omega)\hat{I}_j(\Omega')\rangle = \delta(\Omega-\Omega')\langle \hat{I}_j(\Omega)\rangle + \langle \hat{I}_j(\Omega)\rangle\langle \hat{I}_j(\Omega')\rangle + \left|G_j^{(1)}(\Omega,\Omega')\right|^2, \quad (42)$$

where $\langle \hat{I}_j(\Omega)\rangle = G_j^{(1)}(\Omega,\Omega)$. This relation is typical of thermal-like light, and is a consequence of the Gaussian nature of the field statistics, when the linear transformation (9) is applied to the vacuum state. As it is well known, in fact the marginal distributions of the signal-idler light generated from vacuum are in general thermal-like. We remark that in the low-gain $g \ll 1$, the dominant term is the first one, i.e., the "shot-noise" term δ correlated in frequencies.

$$\langle \hat{I}_j(\Omega)\hat{I}_j(\Omega')\rangle \overset{g\ll 1}{\approx} \delta(\Omega-\Omega')\langle \hat{I}_j(\Omega)\rangle. \quad (43)$$

Therefore, the statistics of photon counts in each arm is Poissonian, in accordance with the result that can be obtained with the biphoton state (12) (see Appendix B for a discussion).

In the following we shall illustrate the three relevant cases. The coherence functions will be evaluated both numerically (Fig. 5) and analytically. In the first case, the complete Sellmeier relations [19] will be used to compute the integrals in (40) and (41), while the linear approximation for phase matching will be exploited to derive approximated analytical formulas.

(i) Limit of a CW pump

Figure 5(a) shows an example of the signal and idler coherence functions in the plane (Ω,Ω'), numerically computed in the case of a long pump pulse $\tau_p \simeq 14\tau'_{gvs}$.

In the limit $\tau_p \gg \tau'_{gvs}$, approximated expressions for the coherence functions can be calculated by inserting the formulas for the biphoton correlation (22) and (23), valid in this

limit, into Eqs. (40) and (41), respectively, and performing the simple integrals. After some passages,

$$G_i^{(1)}(\Omega,\Omega') \simeq G_s^{(1)}(\Omega,\Omega'), \tag{44}$$

$$\xrightarrow{\tau_p \gg \tau'_{gvs}} \tilde{\mathcal{I}}_p(\Omega'-\Omega)\, g^2 \mathrm{sinc}^2\left(\frac{\Omega}{\Omega_{gvs}}\right), \tag{45}$$

where $\tilde{\mathcal{I}}_p(\Omega) = \int \frac{dt}{2\pi} e^{i\Omega t} |\alpha_p(t)/\alpha_p(0)|^2$ is the Fourier transform of the pump intensity profile. These approximated formulas have been checked with the numerical results and show an excellent match. These results may be considered the more refined version of the much simpler CW model analyzed in [11,16], with the narrow peak $\tilde{\mathcal{I}}_p(\Omega'-\Omega)$ being the finite counterpart of the singular Dirac δ appearing in the strictly CW pump model [11].

For a quasi-CW pump the counterpropagating signal and idler photons are predicted to have identical spectral coherence properties. In particular, by looking at the $G^{(1)}$ functions along the diagonal $\Omega' = \Omega$ we see that their spectra $\langle \hat{I}_j(\Omega)\rangle = \langle \hat{A}_j^\dagger(\Omega)\hat{A}_j(\Omega)\rangle$,

$$\langle \hat{I}_s(\Omega)\rangle = \langle \hat{I}_i(\Omega)\rangle \simeq \frac{g^2\tau_p}{\sqrt{2\pi}} \mathrm{sinc}^2\left(\frac{\Omega}{\Omega_{gvs}}\right), \tag{46}$$

are identical and entirely determined by the narrow bandwidth of phase matching Ω_{gvs}. This bandwidth is in turn the inverse of the *long* temporal scale τ_{gvs}, which rules the correlation of the twins. As already remarked, this strongly differs from the copropagating scheme, where the down-conversion bandwidths are huge.

On the other side, when studied as a function of $\Omega'-\Omega$ the $G^{(1)}$ gives the characteristic size of spectral fluctuations, i.e., the spectral *coherence length*. This is determined by the pump bandwidth, more precisely by the width $\sqrt{2}\Delta\Omega_p$ of $\tilde{\mathcal{I}}_p(\Omega'-\Omega)$, which is much narrower than the spectral bandwidths Ω_{gvs}. We can heuristically estimate the number of modes by counting the number of coherence length contained in the spectrum: Therefore, for such a long pulse we expect each signal and idler photon to be generated in a highly incoherent and multimode state, with the number of modes $\propto \frac{\Omega_{gvs}}{\Delta\Omega_p} = \frac{\tau_p}{\tau_{gvs}}$.

(ii) Ultrashort pump pulse

When the pump pulse shorten below the transit time τ'_{gvs} along the crystal slab, the spectral properties of the counterpropagating idler and signal change drastically, becoming strongly asymmetric. First we consider the case of an ultrashort pulse, $\tau_p \ll \tau_{gvm}$ (i.e., such that the pump and the signal tend to split apart during propagation). The asymmetry between the forward- and backward-propagating photons can be clearly appreciated in the third column of Fig. 5, which plots their coherence functions for $\tau_p \approx 0.1\tau_{gvm}$.

Approximated expressions for the coherence functions are derived also in this case, by using the limit behavior of the biphoton correlation described by Eqs. (25) and (26). With some calculations,

$$G_s^{(1)}(\Omega,\Omega') \xrightarrow{\tau_p \ll \tau_{gvm}} \frac{g^2\Omega'_{gvs}}{2}|\tilde{\alpha}_p[\Omega(1-\eta)]|^2 \times \mathrm{sinc}\left(\frac{\Omega'-\Omega}{\Omega_{gvm}}\right) e^{-i\left(\frac{\Omega'-\Omega}{\Omega_{gvm}}\right)}. \tag{47}$$

This formula predicts that the spectrum of the forward-propagating signal,

$$\langle \hat{I}_s(\Omega)\rangle = \frac{g^2\Omega'_{gvs}}{2}|\tilde{\alpha}_p[\Omega(1-\eta)]|^2, \tag{48}$$

is a replica of the pump spectrum with a scale factor $\frac{1}{1-\eta} = \frac{k'_p+k'_i}{k'_i+k'_s}$ on the order unity. The coherence length of the signal (the characteristic size of spectral fluctuations) is instead determined by the width of the narrower sinc function, $l_{coh,s} \approx \Omega_{gvm}$. From this picture we thus expect that the signal photon, when detected independently from its twin, is in a incoherent multimode state, with the number of modes $\propto \frac{\Delta\Omega_p}{(1-\eta)\Omega_{gvm}}$.

In a similar way, for the idler photon we get

$$G_i^{(1)}(\Omega,\Omega') \xrightarrow{\tau_p \ll \tau_{gvm}} \frac{g^2\Omega_{gvm}}{2}\left|\tilde{\alpha}_p\left[-\Omega\frac{1-\eta}{\eta}\right]\right|^2 \times \mathrm{sinc}\left(\frac{\Omega'-\Omega}{\Omega'_{gvs}}\right) e^{-i\left(\frac{\Omega'-\Omega}{\Omega'_{gvs}}\right)}. \tag{49}$$

This formula predicts an idler bandwidth much narrower than the pump; precisely it predicts that the idler spectrum follows the pump spectrum with a scale factor $\frac{\eta}{1-\eta} = \frac{k'_p-k'_s}{k'_i+k'_s} \ll 1$. The coherence length of the idler is $l_{coh,i} \approx \Omega'_{gvs}$, so that the number of temporal modes is predicted to scale as $\frac{\eta\Delta\Omega_p}{(1-\eta)\Omega'_{gvs}} = \frac{\Delta\Omega_p}{(1-\eta)\Omega_{gvm}}$, which is the same number as for the signal (as it must be because the signal and idler are the two members of the same entangled state, and their reduced states must exhibit the same Schmidt dimensionality; see next section).

Notice that this particular scaling of the bandwidths of the forward- and backward-propagating waves with the pump bandwidth is well known in the literature concerning the MOPO. There, the same scaling factors, $\frac{k'_p+k'_i}{k'_i+k'_s}$ for the forward-propagating signal and $\frac{k'_p-k'_s}{k'_i+k'_s}$ for the backward-propagating idler, are predicted to occur [7,8], by using arguments based on the phase-matching characteristic of the process. Here, however, the analysis concerns the quantum properties of the single photons generated well below the MOPO threshold. Moreover, at difference with the classical analysis in [7], such a scaling with the pump spectrum is predicted only in rather extreme conditions, corresponding to an ultrashort pump pulse $\tau_p \ll \tau_{gvm}$. Notice that this limit imposes a precise and not trivial constraint on the minimum observable bandwidth of the idler photon: The behavior described by Eq. (49) is indeed realized only for $\tau_p \ll \tau_{gvm}$, or for $\Delta\Omega_p \gg \Omega_{gvm}$, so that it requires that the idler bandwidth,

$$\delta\Omega_i \simeq \frac{\eta}{1-\eta}\Delta\Omega_p \gg \frac{\eta}{1-\eta}\Omega_{gvm} = \Omega_{gvs}. \tag{50}$$

(iii) Intermediate pump pulse

When $\tau_{gvm} \ll \tau_p \ll \tau'_{gvs}$, the properties of the twin photons are actually intermediate between the two former cases, with the forward-propagating signal photon replicating the pump spectrum, while the coherence properties of the backward-propagating idler are determined by phase matching. These features are clearly exhibited by the central column Fig. 5(b), which plots a numerically computed example of the coherence functions for $\tau_p = 0.04\tau'_{gvs} \approx 4\tau_{gvm}$, short with respect to the

transit time along the slab, but long enough that GVM does not play a relevant role.

The observed features are a straightforward consequence of the separable form (29) of the biphoton amplitude which holds in this limit. Indeed, by using Eq. (29), in the limit $\tau_p/\tau'_{\rm gvs} \to 0$, $\tau_{\rm gvm}/\tau_{\rm p} \to 0$ we obtain

$$G_s^{(1)}(\Omega,\Omega') \to \frac{g^2\Omega_{\rm gvs}}{2}\tilde{\alpha}_p^*[\Omega(1-\eta)]\tilde{\alpha}_p[\Omega'(1-\eta)], \quad (51)$$

$$G_i^{(1)}(\Omega,\Omega') \to \frac{g^2\tau_{\rm p}}{\sqrt{2\pi}}\mathrm{sinc}\left(\frac{\Omega}{\Omega_{\rm gvs}}\right)\mathrm{sinc}\left(\frac{\Omega'}{\Omega_{\rm gvs}}\right)e^{i\frac{\Omega'-\Omega}{\Omega'_{\rm gvs}}}. \quad (52)$$

Thus in this case the signal spectrum is a replica of the broad pump spectrum $I_s(\Omega) \propto |\tilde{\alpha}_p[\Omega(1-\eta)]|^2$, while the idler spectrum is determined by the much narrower phase-matching function $I_i(\Omega) \propto \mathrm{sinc}^2(\frac{\Omega}{\Omega_{\rm gvs}})$. Precisely, the signal spectrum is described by the same formula (48) as in the ultrashort pump case, while the idler spectral properties are described by the same formula (46) that holds in the CW pump limit. However, notice that in the present case the coherence properties are remarkably different, as the two coherence functions are perfectly symmetrical along the two diagonals $\Omega \pm \Omega'$: As can be easily inferred from Eqs. (51) and (52) the two coherence lengths are $l_{{\rm coh},s} \approx \Delta\Omega_{\rm p}$ and $l_{{\rm coh},i} \approx \Omega_{\rm gvs}$, i.e., they are equal to the respective spectral widths. This is in accordance with the separability of the biphoton state, which corresponds to single-mode, almost coherent reduced states for each of the two twin photons taken separately.

We conclude this section observing that the results of (46), (50), and (52) imply that in any pumping regime the idler bandwidth cannot be narrower than the phase-matching bandwidth $\Omega_{\rm gvs}$, a limitation that arises from the imperfect momentum conservation due to the finite length of the crystal slab.

VI. SCHMIDT NUMBER OF ENTANGLEMENT

So far our considerations about the number of modes and the degree of entanglement of the system have been qualitative. A quantitative measure of the entanglement is offered by the so-called Schmidt number [20,21], which is recognized to give an estimate of the number of Schmidt modes participating in the entangled state, i.e., of the effective dimensionality of the entanglement [22]. First of all, as usual, we consider the state conditioned to a photon count,

$$|\phi_{\rm C}\rangle = \int d\Omega_s d\Omega_i \psi(\Omega_s,\Omega_i)\hat{a}_s^\dagger(\Omega_s)\hat{a}_i^\dagger(\Omega_i)|0\rangle, \quad (53)$$

where with respect to the true output state (12), the vacuum term has been dropped. Then, we introduce the Schmidt number, as the inverse of the purity of the state of each separate subsystem,

$$\mathcal{K} = \frac{1}{\mathrm{Tr}\{\rho_s^2\}} = \frac{1}{\mathrm{Tr}\{\rho_i^2\}}, \quad (54)$$

where ρ_s, ρ_i are the reduced density matrix of the signal and idler, e.g., $\rho_s = \mathrm{Tr}_i\{|\phi_{\rm C}\rangle\langle\phi_{\rm C}|\}$. For a two-particle state of the form (53), the Schmidt number can be calculated via an integral formula, as, e.g., derived in [17] (see also [4]),

$$\mathcal{K} = \frac{\mathcal{N}^2}{B}, \quad (55)$$

where

$$\mathcal{N} = \int d\Omega\, G_s^{(1)}(\Omega,\Omega) = \int d\Omega\, G_i^{(1)}(\Omega,\Omega), \quad (56)$$

$$B = \int d\Omega \int d\Omega' \left|G_s^{(1)}(\Omega,\Omega')\right|^2 = \int d\Omega \int d\Omega' \left|G_i^{(1)}(\Omega,\Omega')\right|^2. \quad (57)$$

As can be easily checked, $\mathcal{N}$ is the expectation value of the photon number operator $\hat{N}_j = \int d\Omega \hat{I}_j(\Omega)$ in either the signal or idler arm,

$$\mathcal{N} = \langle\hat{N}_s\rangle = \langle\hat{N}_i\rangle. \quad (58)$$

The quantity at the denominator can be linked to the second-order moment of the photon number. By using Eq. (42) (valid within the field formalism), and integrating it over the two spectral arguments,

$$\int d\Omega \int d\Omega' \left|G_j^{(1)}(\Omega,\Omega')\right|^2 = \langle{:}\hat{N}_j^2{:}\rangle - \langle\hat{N}_j\rangle^2, \quad (59)$$

where $::$ indicates normal ordering, and $j = s,i$. In terms of the normalized $g^{(2)}$ coefficient,

$$g^{(2)} = \frac{\langle{:}\hat{N}_j^2{:}\rangle}{\langle\hat{N}_j\rangle^2} = 1 + \frac{1}{\mathcal{K}}. \quad (60)$$

As recognized in [23,24], the Schmidt number can thus be related to measurable statistical properties of light. In particular, formula (60) is well known to describe the statistics of multimode thermal light, with $\mathcal{K}$ playing the role of the effective number of independent modes in a thermal beam.

Figure 6 shows our results for the Schmidt number. The solid lines plot the "exact" results, where $\mathcal{K}$ has been calculated by numerically performing the integrals involved in (56) and (57), with the phase-matching calculated via the complete Sellmeier relations. The red dashed lines in Figs. 6(a) and 6(b) are asymptotic behaviors, analytically derived by exploiting the linear approximation for phase matching. In particular, by using the approximated formula (45) for the coherence function, and performing the integrals involved in (56) and (57), one obtains the limit of the Schmidt number for a long pump pulse,

$$\mathcal{K} \overset{\tau_p \gg \tau'_{\rm gvs}}{\longrightarrow} \frac{3}{2}\sqrt{\frac{\pi}{2}}\frac{\Omega'_{\rm gvs}}{\Delta\Omega_p}. \quad (61)$$

For an ultrashort pump pulse, the asymptotic behavior of $\mathcal{K}$ is calculated by using formula (49) or (47), for either the signal or the idler coherence function (identical results are indeed obtained). In this case,

$$\mathcal{K} \overset{\tau_p \ll \tau_{\rm gvm}}{\longrightarrow} \frac{1}{1-\eta}\sqrt{\frac{2}{\pi}}\frac{\Delta\Omega_p}{\Omega_{\rm gvm}}. \quad (62)$$

The calculated asymptotes are well in accordance with our qualitative estimates of the number of modes in Sec. V, based

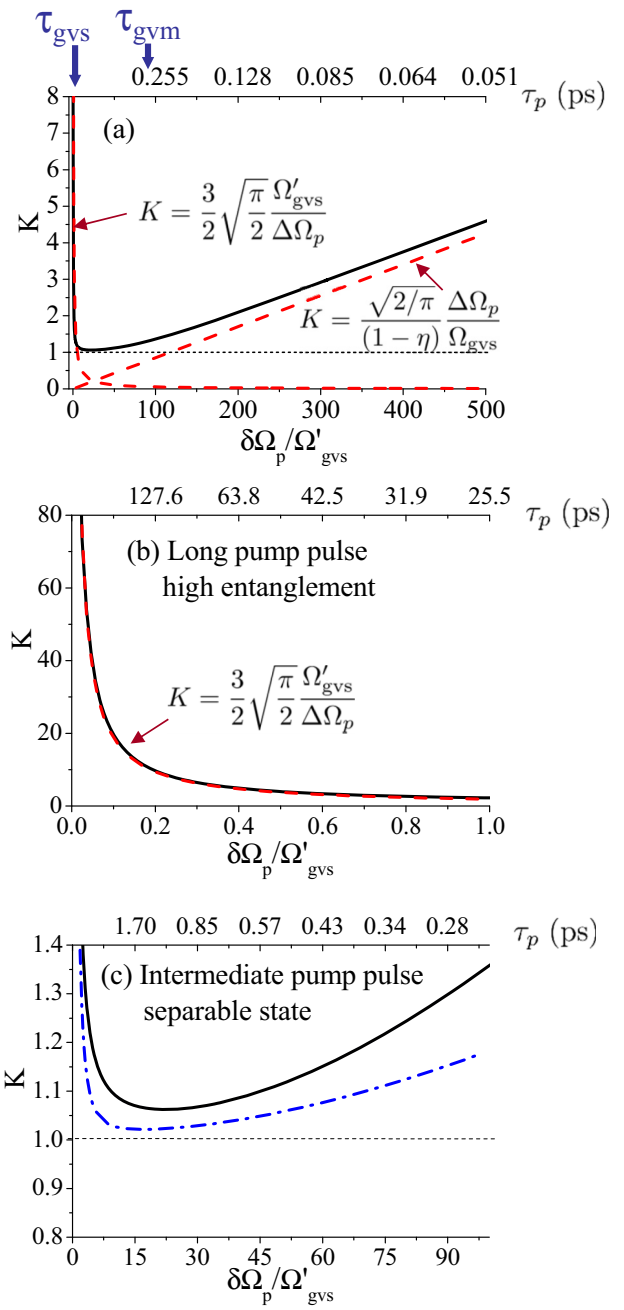

FIG. 6. (Color online) (a) Schmidt number, as a function of the pump spectral bandwidth (lower axis) or duration (upper axis). (b) and (c) Insets of (a), showing the transition from high entanglement for a long pump $\tau_p \gg \tau'_{\rm gvs}$ to an almost separable state for $\tau'_{\rm gvs} \gg \tau_p \gg \tau_{\rm gvm}$. The red dashed lines in (a) and (b) are the calculated asymptotic behaviors; the blue dash-dot line in (c) is the result of a Gaussian approximation. 4-mm PPKTP **A** in Fig. 2, with $\tau'_{\rm gvs} = 25.5$ ps $\tau_{\rm gvm} = 0.27$ ps,; other parameters as in Fig. 3.

on the ratio between the spectral bandwidth and the coherence length.

This shape of the curve, showing a minimum of $\mathcal{K}$ for a given value of the pump bandwidth and linear asymptotes at small and large values of the bandwidth, is commonplace, with a qualitatively similar curve characterizing also the co-propagating case in either temporal [4] or spatial [25] or even spatio-temporal [17] domains. The novelty here is that the minimum value of $\mathcal{K}$ is very close to unity, and remains close to unity for a rather large range of $\Delta\Omega_p$ [see Fig. 6(c)]. This represents indeed a big difference compared to the co-propagating case, where in order to generate separable biphotons very special matching conditions have to be chosen, corresponding to a zero group velocity mismatch between the pump and one of the twin photons, which can be realized only in type II interactions [13,26].

In the backward-propagating case the conditions for separability are very easily approached, and rely entirely on the fact that $\eta = \tau_{\rm gvm}/\tau'_{\rm gvs}$ is naturally a very small quantity, because the temporal separations $\tau_{\rm gvm}, \tau'_{\rm gvs}$ between the co-propagating and the counterpropagating waves are on well-separated time scales.

Indeed, a more refined calculation shows that the minimum value of $\mathcal{K}$, reached for a pump duration intermediate between $\tau_{\rm gvm}$ and $\tau'_{\rm gvs}$ is $K_{\rm min} = 1 + O(\eta)$. This is also confirmed by analytical calculations of the Schmidt number, reported in detail elsewhere [27], performed by means of a Gaussian approximation of the sinc function of phase matching, similarly to what was done in [26]. These calculations [plotted as the blue dash-dot line in Fig. 6(c)] show that the minimum of $\mathcal{K}$ is

$$\mathcal{K}_{\rm min} = \frac{1+\eta}{1-\eta} \approx 1 + 2\eta, \tag{63}$$

reached for $\Delta\Omega_p = \sqrt{3\Omega'_{\rm gvs}\Omega_{\rm gvm}}$. This result suggests that a higher degree of purity of the reduced states can be achieved as the GVM between the two forward propagating is reduced. This is confirmed by the examples in Fig. 7, which compares different crystals and phase-matching conditions. Notice that a small GVM corresponds to a higher degree of purity, as in the

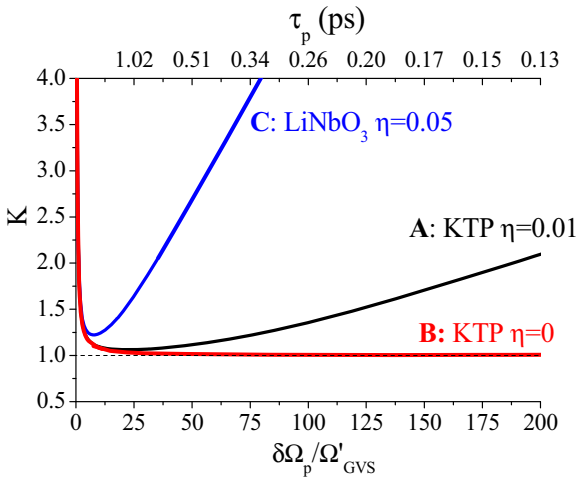

FIG. 7. (Color online) Role of GVM in determining the purity of the state. Schmidt number for different crystals and/or different phase-matching conditions, corresponding to the points **A**, **B**, **C** in Fig. 2. **(A)** 4-mm KTP with $\tau_{\rm gvm} = 0.27$ ps, $\tau'_{\rm gvs} = 25.5$ ps, $\rightarrow \eta = 0.01$ (same as in Figs. 3–6). **(B)** 4-mm KTP, with $\tau_{\rm gvm} = 0$, $\tau'_{\rm gvs} = 24.7$ ps, $\rightarrow \eta = 0$. **(C)** 4-mm $LiNbO_3$ with $\tau_{\rm gvm} = 1.68$ ps, $\tau'_{\rm gvs} = 31.2$ ps, $\rightarrow \eta = 0.05$.

co-propagating case, but that in the present case the condition for separability is much less demanding, as it does not require a vanishing GVM, but just that $\tau_{\rm gvm}$ is small compared to the sum of the inverse of group velocities $\tau'_{\rm gvs}$, which is always verified to some extent.

VII. CONCLUSIONS

In this work we provided a detailed theoretical analysis of the effect of the pump spectral properties on the quantum correlation of counterpropagating photons generated by SPDC in a periodically poled crystal.

In particular, for increasing spectral bandwidths of the pump (decreasing pump durations), we demonstrated a remarkable transition from a high-dimensional entangled state, to an almost separable state. The transition occurs when the pulse duration shortens below the characteristic transit time $\tau_{\rm gvs} = \frac{l_c}{2v_{gs}} + \frac{l_c}{2v_{gi}} \approx \frac{l_c}{2v_{gp}} + \frac{l_c}{2v_{gi}}$ of light along the crystal slab. This *long* temporal scale is a unique characteristic of the counterpropagating geometry, being associated with the delay between the times at which the counterpropagating photons, generated at some point along the slab, appear at their exit faces. The temporal correlation (temporal entanglement) is again restored for pump durations below the *short* temporal delay occurring between the co-propagating waves because of their different group velocities.

The natural existence of such separated time scales ensures the possibility of generating the high purity single photon (i.e., a separable two-photon state), under very general conditions, which differs drastically from the usual co-propagating geometry [13].

These conclusions have been supported through the paper by the analysis of the Schmidt number in Sec. VI, and by analytical and numerical evaluations of the spectral and temporal correlation function (Secs. III and IV).

The study of the marginal statistics of photons in Sec. V has revealed several nontrivial features.

While for a long pump pulse twin photons have the same spectrum and the same coherence properties, in the regime of separability they exhibit very different features. In particular, the properties of the counterpropagating idler are entirely determined by the phase matching in the medium, so that we can say that they reflect the momentum conservation in the process. On the other side, the spectro-temporal properties of the signal are a replica of those of the co-propagating pump laser pulse, and rather reflect the energy conservation.

For an ultrashort pump pulse, our quantum analysis has retrieved results analog to what was predicted in the classical description of the MOPO [7,8], but with some additional limitation. At difference with the MOPO prediction [7], our results impose a precise inferior limit to the observable bandwidth of the backward idler photon, which cannot be narrower than the phase-matching bandwidth $\Omega_{\rm gvs}$. Clearly, our analysis is limited to SPDC, but we notice that, to our knowledge, measurements of the spectrum of the backward wave in the MOPO have been limited by the spectrometer resolution [9], so that our findings may open a question about the effective bandwidth of the backward wave.

APPENDIX A: APPROXIMATIONS FOR THE BIPHOTON AMPLITUDE

In this appendix we derive the approximated forms of the biphoton amplitude used in the text, which holds in the various pump regimes. In all the cases we make use of the linear approximation for phase matching (15), based on the assumption that the bandwidths in play are narrow so that dispersion can be neglected. Under this approximation, the general expression (10) of the biphoton amplitude becomes

$$\psi(\Omega_s,\Omega_i) = \frac{g}{\sqrt{2\pi}}\tilde{\alpha}_p(\Omega_s+\Omega_i)V\left(\frac{\Omega_s}{\Omega_{\rm gvm}} + \frac{\Omega_i}{\Omega'_{\rm gvs}}\right), \quad \text{(A1)}$$

where for brevity of notation we introduced the phase-matching function $V(s) = \mathrm{sinc}(s)e^{is}$.

We consider first the limit of a CW pump (21). Since the pump bandwith is much narrower than the bandwidths $\Omega'_{\rm gvs}$ and $\Omega_{\rm gvm}$ of phase matching, the presence of the pump Fourier amplitude term forces $\Omega_s = -\Omega_i$ into the phase-matching function. As a result,

$$\lim_{\tau_p/\tau'_{\rm gvs}\to\infty} \psi(\Omega_s,\Omega_i)$$

$$= \frac{g}{\sqrt{2\pi}}\tilde{\alpha}_p(\Omega_s+\Omega_i)V\left(-\frac{\Omega_s}{\Omega_{\rm gvs}}\right) \quad \text{(A2)}$$

$$= \frac{g}{\sqrt{2\pi}}\tilde{\alpha}_p(\Omega_s+\Omega_i)V\left(\frac{\Omega_i}{\Omega_{\rm gvs}}\right), \quad \text{(A3)}$$

where we used the relation $1/\Omega_{\rm gvs} = 1/\Omega'_{\rm gvs} - 1/\Omega_{\rm gvm}$, according to the definitions (16)–(18).

The limit (24) of an ultrashort pump is also straightforward. In this case the bandwidths of phase matching are assumed to be much narrower than the pump bandwidth $\Omega'_{\rm gvs} \ll \Omega_{\rm gvm} \ll \Delta\Omega_{\rm p}$, so that the phase-matching function has a narrow peak, which on the slow scale of variation of the pump forces $\Omega_i = -\eta\Omega_s$, or $\Omega_s = -\Omega_i/\eta$ inside the pump argument. Therefore,

$$\lim_{\frac{\tau_p}{\tau_{\rm gvm}}\to 0} \psi(\Omega_s,\Omega_i)$$

$$= \frac{g}{\sqrt{2\pi}}\tilde{\alpha}_p[\Omega_s(1-\eta)]V\left(\frac{\Omega_s}{\Omega_{\rm gvm}} + \frac{\Omega_i}{\Omega'_{\rm gvs}}\right) \quad \text{(A4)}$$

$$= \frac{g}{\sqrt{2\pi}}\tilde{\alpha}_p\left[-\Omega_i\frac{1-\eta}{\eta}\right]V\left(\frac{\Omega_s}{\Omega_{\rm gvm}} + \frac{\Omega_i}{\Omega'_{\rm gvs}}\right). \quad \text{(A5)}$$

The intermediate pump limit (28) where $\Omega'_{\rm gvs} \ll \Delta\Omega_{\rm p} \ll \Omega_{\rm gvm}$ is a bit more involved. We remind one that the existence of this limit also requires $\eta = \Omega'_{\rm gvs}/\Omega_{\rm gvm} \ll 1$, which is in practice always verified to some extent. By introducing the pump frequency $\Omega_p = \Omega_s + \Omega_i$, we recast the argument of the sinc function,

$$\frac{\Omega_s}{\Omega_{\rm gvm}} + \frac{\Omega_i}{\Omega'_{\rm gvs}} = \frac{\Omega_p}{\Omega_{\rm gvm}} + \Omega_i\left(\frac{1}{\Omega'_{\rm gvs}} - \frac{1}{\Omega_{\rm gvm}}\right) \approx \frac{\Omega_i}{\Omega_{\rm gvs}}, \quad \text{(A6)}$$

where the term $\Omega_p/\Omega_{\rm gvm}$ has been neglected because it is on the order $\Delta\Omega_{\rm p}/\Omega_{\rm gvm} \ll 1$.

Concerning the pump amplitude we recast it as

$$\tilde{\alpha}_p(\Omega_s+\Omega_i) = \tilde{\alpha}_p\left[\Omega_s(1-\eta) + \left(\frac{\Omega_s}{\Omega_{\rm gvm}} + \frac{\Omega_i}{\Omega'_{\rm gvs}}\right)\Omega'_{\rm gvs}\right]$$

$$\approx \tilde{\alpha}_p[\Omega_s(1-\eta)], \quad \text{(A7)}$$

where the approximation in the second line holds because $(\frac{\Omega_s}{\Omega_{\rm gvm}} + \frac{\Omega_i}{\Omega'_{\rm gvs}})$ is the argument of the sinc function [see Eq. (A1)], so that it is limited to values inside the bandwidth of the sinc, say on the order $\simeq 10$. Provided that $\Omega'_{\rm gvs}/\Delta\Omega_{\rm p}$ is small enough, this term becomes therefore negligible. With this in mind we can write the limiting behavior of the biphoton amplitude:

$$\lim_{\substack{\tau_p/\tau'_{\rm gvs}\to 0 \\ \tau_{\rm gvm}/\tau_{\rm p}\to 0}} \psi(\Omega_s,\Omega_i)$$

$$= \frac{g}{\sqrt{2\pi}}\tilde{\alpha}_p[\Omega_s(1-\eta)]e^{i\frac{\Omega_s}{\Omega_{\rm gvm}}}\,\mathrm{sinc}\left(\frac{\Omega_i}{\Omega_{\rm gvs}}\right)e^{i\frac{\Omega_i}{\Omega_{\rm gvs}}}$$

$$\approx \frac{g}{\sqrt{2\pi}}\tilde{\alpha}_p[(\Omega_s)e^{i\frac{\Omega_s}{\Omega_{\rm gvm}}}\,\mathrm{sinc}\left(\frac{\Omega_i}{\Omega_{\rm gvs}}\right)e^{i\frac{\Omega_i}{\Omega_{\rm gvs}}}, \tag{A8}$$

where the approximation in the last line is not mandatory, but could be useful in order to get consistent results, because this limit can be realized only for $\eta = \tau_{\rm gvm}/\tau'_{\rm gvs} \to 0$.

APPENDIX B: RELATION BETWEEN THE STATE AND THE FIELD FORMALISMS

This appendix briefly discusses the relation between the low-gain field formalism (9) and the formalism of the biphoton state (12). The following arguments apply to any PDC process in the low gain.

In particular, we consider the input-output relations (9), which represent the perturbative solution of the field propagation equations (3), correct up to first order in the parametric gain $g \ll 1$. The transformation (9) can be recast as

$$\hat{a}_j^{\rm out}(\Omega) = \hat{R}^\dagger \hat{a}_j(\Omega)\hat{R} \quad (j = s,i), \tag{B1}$$

where $\hat{a}_j$ are the input operators (for brevity of notation we omitted the "in" superscript),

$$\hat{R} = \exp\left\{\int d\Omega_s d\Omega_i [\psi(\Omega_s,\Omega_i)\hat{a}_s^\dagger(\Omega_s)\hat{a}_i^\dagger(\Omega_i) - \psi^*(\Omega_s,\Omega_i)\hat{a}_s(\Omega_s)\hat{a}_i(\Omega_i)]\right\}, \tag{B2}$$

and it is meant that only zero and first order in g have to be retained in the transformation (B1).

Conversely, by applying the generator of the transformation (B1) to the input vacuum state and retaining only terms up to first order in g, one gets

$$|\phi\rangle_{\rm out} = \hat{R}|0\rangle \tag{B3}$$

$$\simeq \left[\hat{1} + \int d\Omega_s d\Omega_i \psi(\Omega_s,\Omega_i)\hat{a}_s^\dagger(\Omega_s)\hat{a}_i^\dagger(\Omega_i)\right]|0\rangle, \tag{B4}$$

which is the biphoton state (12).

The second procedure, however, does not produce entirely equivalent results. To be precise, it produces equivalent results for second-order moments of field operators. As can be easily verified, the biphoton correlation $\langle \hat{a}_s(\Omega_s)\hat{a}_i(\Omega_i)\rangle$ and the coherence function $\langle \hat{a}_j^\dagger(\Omega)\hat{a}_j(\Omega')\rangle$ calculated with the output state (B4) are the same as those calculated within the field formalism, displayed in formulas (13), and (40) and (41), respectively.

However, some differences arise for higher order moments. Let us consider, for example, the autocorrelation of intensities in each signal-idler arm. The field approach gives the thermal-like formula (42), while the calculation with the biphoton state gives only the shot noise term of Eq. (43). For $g \to 0$ the two results asymptotically coincide. However, when considering the normally ordered part of the correlation, in the field formalism,

$$\langle : \hat{I}_j(\Omega)\hat{I}_j(\Omega') : \rangle = \langle \hat{I}_j(\Omega)\rangle\langle \hat{I}_j(\Omega')\rangle + \left|G_j^{(1)}(\Omega,\Omega')\right|^2, \tag{B5}$$

while with the biphoton state,

$$\langle : \hat{I}_j(\Omega)\hat{I}_j(\Omega') : \rangle = 0. \tag{B6}$$

These differences arise from the truncation at first order in g: In the field formalism it leaves the possibility of generating multiple photon pairs, although with a smaller and smaller probability. As a result, the marginal statistics of each beam is the thermal statistics corresponding to a very low mean photon number, where the probability of having more than one signal or idler photon is small but not zero. Conversely, the truncation at first order on the state has a more drastic effect, leaving only a two-photon state, for which the probability of having more than one photon in each arm is exactly zero, which implies relation (B6).

[1] C. K. Hong, Z. Y. Ou, and L. Mandel, Measurement of Subpicosecond Time Intervals between Two Photons by Interference, Phys. Rev. Lett. **59**, 2044 (1987).

[2] A. Gatti, E. Brambilla, L. Caspani, O. Jedrkiewicz, and L. A. Lugiato, *X* Entanglement: The Nonfactorable Spatiotemporal Structure of Biphoton Correlation, Phys. Rev. Lett. **102**, 223601 (2009).

[3] O. Jedrkiewicz, J.-L. Blanchet, E. Brambilla, P. Di Trapani, and A. Gatti, Detection of the Ultranarrow Temporal Correlation of Twin Beams via Sum-Frequency Generation, Phys. Rev. Lett. **108**, 253904 (2012).

[4] Y. M. Mikhailova, P. A. Volkov, and M. V. Fedorov, Biphoton wave packets in parametric down-conversion: Spectral and temporal structure and degree of entanglement, Phys. Rev. A **78**, 062327 (2008).

[5] M. Avenhaus, M. V. Chekhova, L. A. Krivitsky, G. Leuchs, and C. Silberhorn, Experimental verification of high spectral entanglement for pulsed waveguided spontaneous parametric down-conversion, Phys. Rev. A **79**, 043836 (2009).

[6] S. E. Harris, Proposed backward wave oscillation in the infrared, Appl. Phys. Lett. **9**, 114 (1966).

[7] C. Canalias and V. Pasiskevicius, Mirrorless optical parametric oscillators, Nature Photonics **1**, 459 (2007).

[8] G. Strmqvist, V. Pasiskevicius, C. Canalias, P. Aschieri, A. Picozzi, and C. Montes, Temporal coherence in mirrorless

optical parametric oscillators, J. Opt. Soc. Am. B **29**, 1194 (2012).

[9] V. Pasiskevicius, G. Strmqvist, F. Laurell, and C. Canalias, Quasi-phase matched nonlinear media: Progress towards nonlinear optical engineering, Optical Materials **34**, 513 (2012).

[10] Y. J. Ding and J. B. Khurgin, Backward Optical Parametric Oscillators and Amplifiers, IEEE J. of Quantum Electronics **32**, 1574 (1996).

[11] T. Corti, E. Brambilla, and A. Gatti, Critical behaviour of coherence and correlation of counter-propagating twin beams (unpublished).

[12] A. Christ, A. Eckstein, P. J. Mosley, and C. Silberhorn, Pure single photon generation by type-IPDC with backward-wave amplification, Opt. Expr. **17**, 3441 (2009).

[13] P. J. Mosley, J. S. Lundeen, B. J. Smith, P. Wasylczyk, A. B. U'Ren, C. Silberhorn, and I. A. Walmsley, Heralded Generation of Ultrafast Single Photons in Pure Quantum States, Phys. Rev. Lett. **100**, 133601 (2008); P. J. Mosley, J. S. Lundeen, B. J. Smith, and I. A. Walmsley, Conditional preparation of single photons using parametric down-conversion: A recipe for purity, New J. Phys. **10**, 093011 (2008).

[14] R. W. Boyd, in *Nonlinear Optics*, 3rd ed. (Elsevier, Amsterdam, 2008), Chap. 2, p. 84.

[15] E. Brambilla, O. Jedrkiewicz, P. Di Trapani, and A. Gatti, Space-time coupling in upconversion of broadband down-converted light, J. Opt. Soc. Am. B **31**, 1383 (2014).

[16] T. Suhara and M. Ohno, Quantum Theory Analysis of Counterpropagating Twin Photon Generation by Parametric Downconversion, IEEE J. of Quantum Electronics **46**, 1739 (2010).

[17] A. Gatti, E. Brambilla, T. Corti, and D. M. Horoshko, Dimensionality of the spatio-temporal entanglement of PDC photon pairs, Phys. Rev. A **86**, 053803 (2012).

[18] M. C. Booth, M. Atature, G. Di Giuseppe, A. V. Sergienko, B. E. A. Saleh, and M. C. Teich, Counterpropagating entangled photons from a waveguide with periodic nonlinearity, Phys. Rev. A **66**, 023815 (2002).

[19] D. Nikogosyan, *Nonlinear Optical Crystals: A Complete Survey* (Springer, New York, 2005).

[20] A. Ekert and P. L. Knight, Entangled quantum systems and the Schmidt decomposition, Am. J. Phys. **63**, 415 (1995).

[21] S. Parker, S. Bose, and M. B. Plenio, Entanglement quantification and purification in continuous-variable systems, Phys. Rev. A **61**, 032305 (2000).

[22] M. P Van Exter, A. Aiello, S. S. R. Oemrawsingh, G. Nienhuis, and J. P. Woerdman, Effect of spatial filtering on the Schmidt decomposition of entangled photons, Phys. Rev. A **74**, 012309 (2006).

[23] K. Laiho, A. Christ, K. N. Cassemiro, and C. Silberhorn, Testing spectral filters as Gaussian quantum optical channels, Opt. Lett **36**, 1476 (2011).

[24] A. Christ, K. Laiho, A. Eckstein, K. N Cassemiro, and C. Silberhorn, Probing multimode squeezing with correlation functions, New J. of Phys. **13**, 033027 (2011).

[25] C. K. Law and J. H. Eberly, Analysis and Interpretation of High Transverse Entanglement in Optical Parametric Down Conversion, Phys. Rev. Lett. **92**, 127903 (2004).

[26] W. P. Grice, A. B. U'Ren, and I. A. Walmsley, Eliminating frequency and space-time correlations in multiphoton states, Phys. Rev. A **64**, 063815 (2001).

[27] E. Brambilla and A. Gatti, The Schmidt number of counter-propagating twin photons (unpublished).